Available online at www.sciencedirect.com
SCIENCE DIRECT®
ELSEVIER
International Journal of Multiphase Flow 30 (2004) 979–994
International Journal of Multiphase Flow
www.elsevier.com/locate/ijmulflow

On the coalescence of gold nanoparticles ☆

S. Arcidiacono [a], N.R. Bieri [a], D. Poulikakos [a,*], C.P. Grigoropoulos [b]

[a] *Laboratory of Thermodynamics in Emerging Technologies, Institute of Energy Technology, Swiss Federal Institute of Technology, ETH Center, ML J 36 , CH-8092 Zurich, Switzerland*
[b] *Laser Thermal Laboratory, Department of Mechanical Engineering, University of California, Berkeley, CA 94720-1740, USA*

Received 25 November 2003; received in revised form 15 March 2004

Abstract

The present work investigates the coalescence process of two gold nanoparticles for a host of initial temperatures and starting radii in vacuum with the help of molecular dynamics (MD) simulations. Diverse mechanisms of the first sintering stage, characterized by a growing neck region, were found. The results are compared with a phenomenological macroscopic model based on an energy balance and supplemented by a model for the surface variation of the nanosystem under consideration. The model is also modified to account for the curvature dependence of the melting temperature of the nanoparticles. Accounting for the findings of the MD simulations for the neck growth rate, the validity of the analytical model with the initial temperature and radius of the particle is shown. The calculations were extended to particles having radii between 9.5 and 25 Å.

Keywords: MD simulation; Gold nanoparticle; Coalescence

☆ It is a pleasure for us to contribute this paper to the Festschrift issue of the International Journal of Multiphase Flow, dedicated to the 65th birthday of Professor George Yadigaroglu. The senior co-authors of the paper (D.P. and C.P.G.) have known "Yadi" for a long time. We have both enjoyed and benefited from his important contributions to the science of multiphase flow, as well as from our interactions at the personal level. It is also befitting that this paper was co-authored by researchers in the two academic institutions (ETH and UCB) where Yadi spent his professional career to date. We wish him well on his 65th birthday and look forward to his future contributions.

* Corresponding author. Tel.: +41-1-6322738; fax: +41-1-632-1176.
E-mail address: dimos.poulikakos@ethz.ch (D. Poulikakos).

0301-9322/$ - see front matter
doi:10.1016/j.ijmultiphaseflow.2004.03.006

1. Introduction

As the utilization of ultrafine particles is becoming increasingly important in industrial applications, including a host of novel manufacturing processes, there is a great interest to understand the basic phenomena, not only in the production, but also in the utilization of such particles under diver thermodynamic conditions. To this end, there are different models developed for ceramics describing the evolution of sintering of equally sized particles based on the neck growth rate (Coblenz et al., 1980) valid in the early sintering stages and often used in numerical simulations (Kobata et al., 1991; Kruis et al., 1993; Shimada et al., 1994). Friedlander and Wu (1994) derived a theory for solid-state diffusion valid for the coalescence stage (intended as the approach of a non-spherical particle to a spherical shape). Zachariah and Carrier (1999) showed, comparing their MD simulations with a phenomenological model, that the results obtained in Friedlander and Wu (1994) could be applied also in the early stage of sintering of silicon nanoparticles. The same authors and Lehtinen and Zachariah (2001, 2002) reported that during the sintering process of two particles the surface area reduction leads to an energy release with a consequent increase of temperature that accelerates the entire process.

Several works compared the sintering process of nanoparticles of different materials both experimentally and theoretically and found good agreement with the "neck" theory (Coblenz et al., 1980). To exemplify, Kobata et al. (1991) investigated the sintering of TiO_2 during gas-phase reaction. Shimada et al. (1994) investigated experimentally the size reduction of fine silver agglomerates by sintering in a heated gas flow. Nakaso et al. (2002) reported that gold agglomerates with small primary particles will compact mainly by the subsequent coalescence of these primary particles.

Xing and Rosner (1999) were able to predict some experimental results for alumina and titania nanoparticles assuming that coalescence occurs via surface diffusion and taking into account the curvature dependence of the surface melting temperature. Tsantilis et al. (2001) suggested a similar approach for the coagulation of silica nanoparticles.

The sintering of two copper nanoparticles via MD was studied in Zhu and Averback (1996a,b). The evaluated diffusion coefficient for the studied sintering event was by a factor of 10^3 larger than the diffusion coefficient for grain boundary diffusion, the expected dominant mechanism. They observed during the early sintering stages an elastic deformation after which a relative rotation between the two particles begins until a low minimum energy grain boundary was reached. The simulation of Cu and Au nanoparticle arrays (Zeng et al., 1998) showed a different sintering mechanism of nanosized particles compared to microsized. Large atomic potential gradients, present where the two surfaces form a cusp at the point of contact, are decreasing the expected temporal scales of the process. Lewis et al. (1997) studied the coalescence of liquid–liquid, solid–liquid and solid–solid gold nanoparticles via MD simulations using the embedded atom method (EAM) potential (Foiles et al., 1986). They found no agreement between the sintering time obtained by their MD results and the classical macroscopic neck theories. The latter were assuming that the leading phenomenon was surface diffusion, but did not account for the energy release due to the surface area reduction and the relative temperature increase of the system. The simulations showed a rapid increase of the neck growth at the beginning, followed by a slow tendency to recover the spherical shape. The simulation of the melting and the coalescence of metallic clusters (Ag, Cu and Pb) of size from 50 to 300 atoms was performed by Mazzone (2000). Size dependence

of the melting temperature and significant differences in the coalescence stage compared with classical theories were reported.

The configuration of a single gold nanoparticle has been studied in the past and results have been reported in the literature. As demonstrated in previous numerical (Ercolessi et al., 1991; Lewis et al., 1997; Chushak and Bartell, 2001; Shim et al., 2002) and experimental (Buffat and Borel, 1976; Lai et al., 1996) works the melting temperature and the latent heat of fusion are dependent on the particle size and are markedly lower than their bulk counterparts. This phenomenon has great significance in technological applications, since partial or complete melting can be obtained at lower temperatures when ultrafine particles of matter are used (Bieri et al., 2002, 2003), enabling the manufacturing of gold nanostructures on temperature sensitive surfaces. Furthermore, a thin liquid shell can be present in a stable configuration around the solid structure even though the particle temperature is below the melting point (Kofman et al., 1994). This morphology can also be predicted by MD simulations (Ercolessi et al., 1991; Lewis et al., 1997) and can have an important effect especially in the early sintering/coalescence stage.

The motivation and main novelty of this work is to achieve a better understanding of the phenomenology and specifics of the coalescence process of gold nanoparticles with the help of MD, by employing a reliable model for the interatomic potentials, which we first test herein again experimental data. A simple macroscopic model is developed and presented in parallel and its predictions vis a vis those of the simulations are discussed. At the same time, contrary to previous MD works, we show that classical "neck" theories, modified to take into account the size dependence of the melting temperature, can predict the first stage of the sintering process also in nanoscales at least for particles that are larger than ≈ 20 Å and temperatures near the corresponding melting point.

2. Model

2.1. Molecular dynamics simulation

The molecular dynamics simulations employed herein to study a wide range of gold nanoclusters, 9.5–25.2 Å (225–3805 atoms), is based on the glue potential (Ercolessi et al., 1988):

$$V = \frac{1}{2}\sum_{ij} \Phi(r_{ij}) + \sum_{i} U(n_i) \tag{1}$$

where r_{ij} is the distance between two atoms, $\Phi(r_{ij})$ is a standard two body potential, $U(n_i)$ is the energy associated with the coordination n_i of the atom i, $n_i = \sum_j \rho(r_{ij})$ is defined as the superposition of contribution from neighbor atoms and $\rho(\boldsymbol{r})$ is a short-ranged monotonically decreasing function of distance. The parameter n_i can be interpreted as the electronic density and the parameter ρ as the electronic density of an isolated atom. The functions $\Phi(\boldsymbol{r})$, $U(\boldsymbol{n})$ and $\rho(\boldsymbol{r})$ are reconstructed empirically in Ercolessi et al. (1988) in order to reproduce the experimental values of gold in a wide range of thermodynamic conditions. The expressions and details on these functions used herein can be found in the above mentioned paper.

The gold nanoparticles were constructed to have a spherical shape with a face centered cubic (fcc) lattice and placed in vacuum. The target system temperature was obtained rescaling every 250 time steps the velocity of each particle with the factor $\chi = (T_{\text{target}}/T)^{1/2}$, where T_{target} is the requested temperature and T is the average instantaneous temperature of the system. The velocity rescaling was applied for $\approx 5\times 10^4$ time steps. After that, the system was equilibrated until no change in the average temperature was observed. Depending on the studied system the equilibration required up to 5×10^6 time steps (for the particles with a temperature near the melting point). The simulation runs were performed for $\approx 10^6$ time steps to collect data to have a good statistics. The chosen time step was 2.86 fs, while the cutoff distance was 3.9 Å for $\rho(\boldsymbol{r})$ and 3.7 Å for $\Phi(\boldsymbol{r})$ (these are intrinsically defined in the glue potential which is considering only the first neighbor atoms).

Some particles were melted and then frozen before the sintering simulation process to obtain a low energy configuration.

In order to simulate the coalescence process, one equilibrated particle and a copy of it were entered into the simulation domain at a distance small enough to be within the interaction range of the intermolecular forces, ≈3 Å. Some of the copied particles were also rotated by 45° to study the influence of the lattice arrangement.

2.2. Analytical model

As a macroscopic alternative, the sintering process can be analyzed with a free energy balance (Lehtinen and Zachariah, 2001, 2002). Considering our system as two gold particles consisting of each N atoms in a vacuum, the total energy E of this system is the sum of the bulk energy E_{bulk} and the surface energy E_{surf}. Any change in the total energy would result from gains or losses to the surrounding. In the present model this change is zero, neglecting radiation and convective losses, to make the comparison with the MD simulation as close as possible. As the two particles coalesce to form one larger particle, the surface of the system is changing. This reduction in the surface area results in an energy release which increases the particle temperature significantly. Since the dynamics of the coalescing process is dependent on temperature, this temperature increase will accelerate the entire process.

The energy change of the system can be written as

$$\frac{\mathrm{d}E}{\mathrm{d}t} = \frac{\mathrm{d}(E_{\text{bulk}} + E_{\text{surface}})}{\mathrm{d}t} = 2NC_{\text{v}}\frac{\mathrm{d}T}{\mathrm{d}t} + \sigma_{\text{sv}}\frac{\mathrm{d}a}{\mathrm{d}t} = 0 \tag{2}$$

where C_{v} is the constant-volume heat capacity, σ_{sv} is the solid–vapor surface tension, T and a are the temperature and the surface of the two coalescing particles at time t.

The surface area reduction by sintering can be described by the linear law of Koch and Friedlander (1990):

$$\frac{\mathrm{d}a}{\mathrm{d}t} = -\frac{1}{\tau}(a - a_{\text{s}}) \tag{3}$$

where a_{s} is the surface area of the final sphere (assumed in the analytical solution) and τ the characteristic sintering time that will be defined later in this section. The relation above was initially derived assuming that the coalescence rate of an agglomerate in the initial state is directly

proportional to its excess surface area [(actual surface area) – (equivalent spherical area)]. This assumption was later shown to be representative also for the final stages of transformation to sphericity for an originally slightly non-spherical particle by Friedlander and Wu (1994).

Finally, the derivative of the particle temperature can be expressed as

$$\frac{\mathrm{d}T}{\mathrm{d}t} = -\frac{\sigma_{\mathrm{sv}}}{2NC_{\mathrm{v}}}\frac{\mathrm{d}a}{\mathrm{d}t} \tag{4}$$

This system (3) and (4) of two dependent differential equations is solved with a Runge Kutta fourth order algorithm.

There exist different mechanisms which can drive the coalescence of two solid nanoparticles such as surface diffusion, grain boundary diffusion, evaporation–condensation, and lattice diffusion. The modeling of the initial stage of sintering expresses the neck growth of two spheres of the same radius (Fig. 1) with a center-to-center approach as

$$\left(\frac{x}{r_{\mathrm{p}}}\right)^{n} = \frac{Bt}{r_{\mathrm{p}}^{m}} \tag{5}$$

where r_{p} is the initial particle radius, x the neck radius, t the time and B a constant depending on the temperature. If grain boundary diffusion or surface diffusion are dominant Eq. (5) becomes (Coblenz et al., 1980):

$$t = \frac{\left(\frac{x}{r_{\mathrm{p}}}\right)^{6} r_{\mathrm{p}}^{4} RT}{CwD\sigma_{\mathrm{sv}}\Omega} \tag{6}$$

where C is a constant, R is the universal gas constant, D is the grain boundary or surface diffusion coefficient, Ω is the molar volume and w is the surface or grain boundary layer width, estimated as $\Omega^{1/3}$ (Kruis et al., 1993). The previously introduced characteristic sintering time τ is defined as the time in Eq. (6) at which the neck radius to particle radius ratio reaches 0.83. This value was found by Kobata et al. (1991) and represents the largest possible neck to radius ratios of two coalescing spheres where no undercutting is visible and it is consistent with that numerically evaluated for an infinite line of spheres sintering into an infinite cylinder ($x/a = 0.817$) and the one of a sphere sintering onto a plane ($x/a = 0.84$) (Nichols and Mullins, 1965).

The diffusion coefficient is assumed to follow the Boltzmann–Arrhenius dependency:

$$D = D_0 \exp(-E_{\mathrm{a}}/RT) \tag{7}$$

where D_0 is the pre-exponential diffusion coefficient and E_{a} the activation energy.

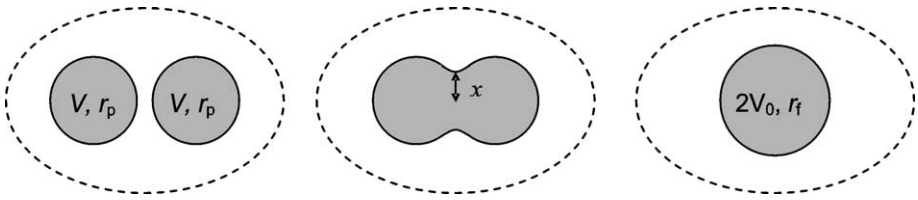

Fig. 1. Sketch of the sintering of two equally sized particles.

Assuming grain boundary diffusion as the driving phenomenon (Nakaso et al., 2002), the proper pre-exponential factor and the activation energy can be calculated with the empirical relationship deduced from experimental data of bulk material valid for fcc crystal structures (Gjostein, 1972):

$$D_0 = 0.3 \text{ cm}^2/\text{s} \tag{8}$$

$$E_a = 47.5 \cdot T_M \text{ J/mol} \tag{9}$$

where T_M is the bulk melting temperature.

The surface tension is calculated using the relation of Murr (1975) for pure fcc metals:

$$\sigma_{sv} \simeq 1.2(\sigma_{lv})_M + 0.45(T_M - T) \tag{10}$$

where $(\sigma_{lv})_M$ is the surface tension of liquid bulk gold at the melting point.

As it will be discussed in detail in the next section, the melting temperature of a nanoparticle T^0 is curvature dependent. In both Eqs. (9) and (10) the value of the bulk melting temperature T_M is replaced by T^0. Furthermore, to account for the changing size from the initial to the final configuration, it is assumed that the starting melting temperature is equal to that corresponding to the initial particle radius and it increases exponentially up to that corresponding to the final radius. The final melting temperature is reached when the curvature is approximately equal to unity.

3. Results

3.1. Single particle

To benchmark the methodology, calculations are first conducted on *single* gold nanoparticles with different radii.

The most common approach to evaluate the melting temperature of a particle via molecular dynamics is to evaluate the point of discontinuity in the potential energy when plotted as a function of the temperature (Fig. 2). The jump in the potential energy is the latent heat of fusion and the corresponding temperature is the melting temperature.

Fig. 3 shows the melting temperatures as a function of the particle radius evaluated from the present calculations and the analytical formulation reported in Buffat and Borel (1976):

$$\ln\frac{T^0}{T_M} = -\frac{2}{\rho_s L}\left(\frac{\rho_s}{\rho_l}\right)^{1/3}\frac{1}{r_s^*}\left\{\sigma_l\left(1-\frac{\rho_s}{\rho_l}\right)+\sigma_{sl}\left[1-\frac{\delta}{r_s^*}\left(\frac{\rho_s}{\rho_l}\right)^{1/3}\right]^{-1}\right\} \tag{11}$$

where σ_{sl} is the solid–liquid interfacial tension, σ_l is the surface tension of the liquid, δ is the liquid-layer thickness, r_s^* is the radius of the particle at the melting point assuming that the particle is in the solid form, ρ_s and ρ_l are, respectively, the solid and liquid densities and L is the latent heat of fusion. The parameters σ_{sl}, σ_l, ρ_s, ρ_l and L used in Eq. (11) correspond to the experimental values of bulk gold while δ and σ_{sl} are the same obtained in Buffat and Borel (1976) fitting their experimental data.

The calculated latent heat as a function of the particle radius is shown in Fig. 4. The solid line is the proposed relation by Lai et al. (1996):

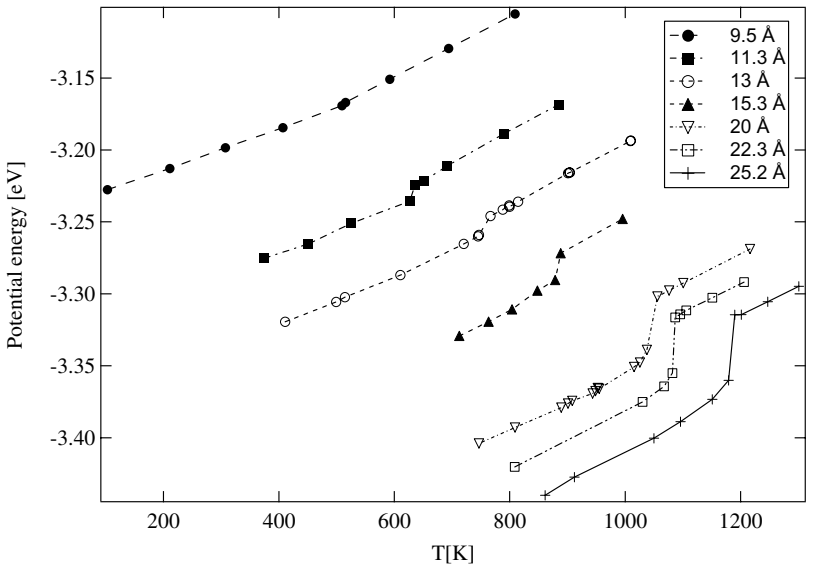

Fig. 2. Single particle calculations: potential energy as a function of the particle temperature for different particle radii.

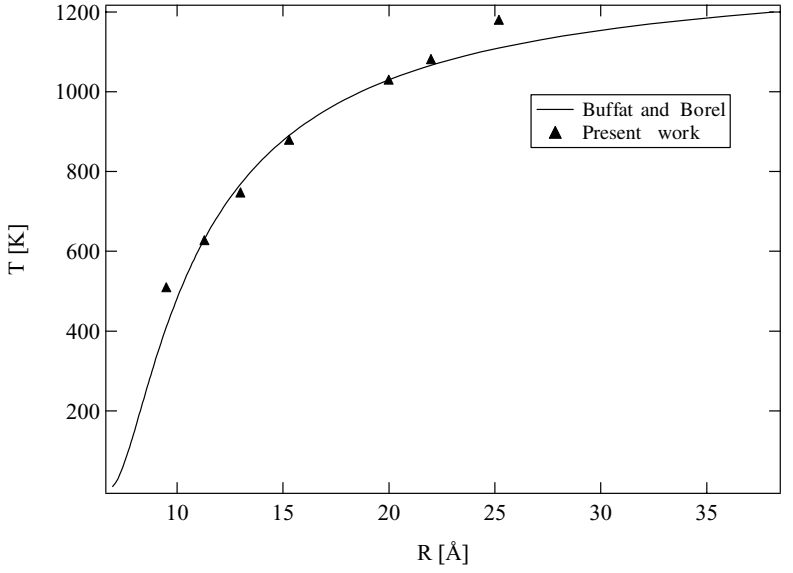

Fig. 3. Single particle: melting temperature as a function of the particle radius and comparison with the results of Buffat and Borel (1976).

$$L_{\mathrm{M}} = L\left(1 - \frac{\delta}{r}\right)^3 \tag{12}$$

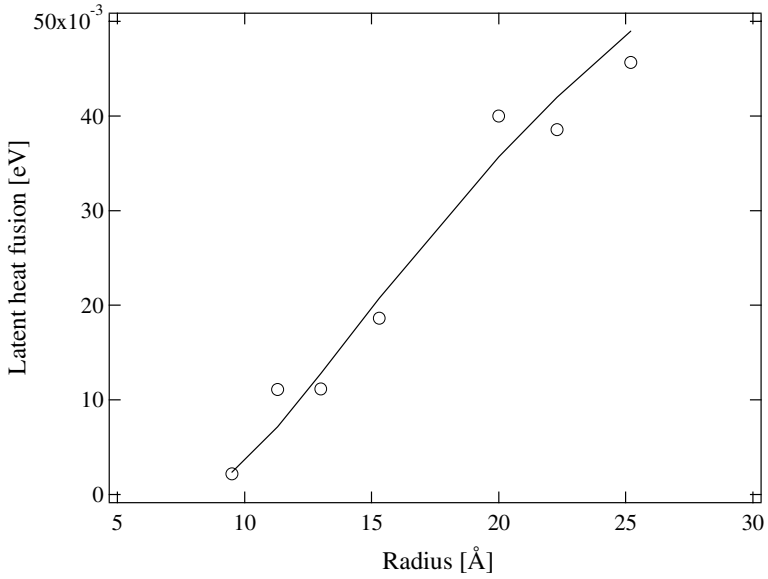

Fig. 4. Single particle: latent heat of fusion as a function of the particle radius. Circles: MD results. Solid line: fitting curve proposed in Lai et al. (1996).

where L_M is the latent heat of fusion for the particle of radius r and δ is a fitting parameter that is a measure of the liquid shell. The obtained value was $\delta \approx 7$ Å that is in agreement with the value reported in Buffat and Borel (1976) for the melting temperature, $\delta \approx 6.2$ Å.

3.2. Two particle coalescence

The time evolution of the gyration radii during the particle coalescence evaluated via MD, defined as $R_\alpha = \frac{1}{N}\sum_{i=1}^{N} \alpha_i^2$, where $\alpha = x, y, z$ are the molecule coordinates and N total number of the simulated molecules, is reported in Fig. 5 for two particles of 20 Å radius and an initial temperature of 895 K. A typical transient can be characterized by two main stages. A very fast first phase can be distinguished where a neck forms between the two particles and its growth rate is following a power law in time (Fig. 6) as given in Eq. (5). This behavior is neither dependent on the particle size nor on the initial temperature. This phase, in present case, is persisting until ≈ 0.3 ns (Figs. 5 and 6). A similar order of magnitude for this time is reported by Lewis et al. (1997) for $r = 16.37$ Å.

The second phase starts when the neck disappears and only one particle is recognized. The gyration radii evolution in this case is much slower. For the present case shown in Fig. 5 an actual sphere shape is not reached within the simulation time although more than 2×10^6 time steps were performed. It is difficult to state whether the final configuration will approach to a perfect spherical shape for this would require a simulation of hundred nanoseconds. As discussed in Herring (1950) and Friedlander and Wu (1994) the dominant mechanism in this phase can be solid-state self diffusion driven by stress gradients resulting from a non-perfect sphericity. In addition, unlike liquids, in solids it is possible to have a non-spherical final shape (non-spherical

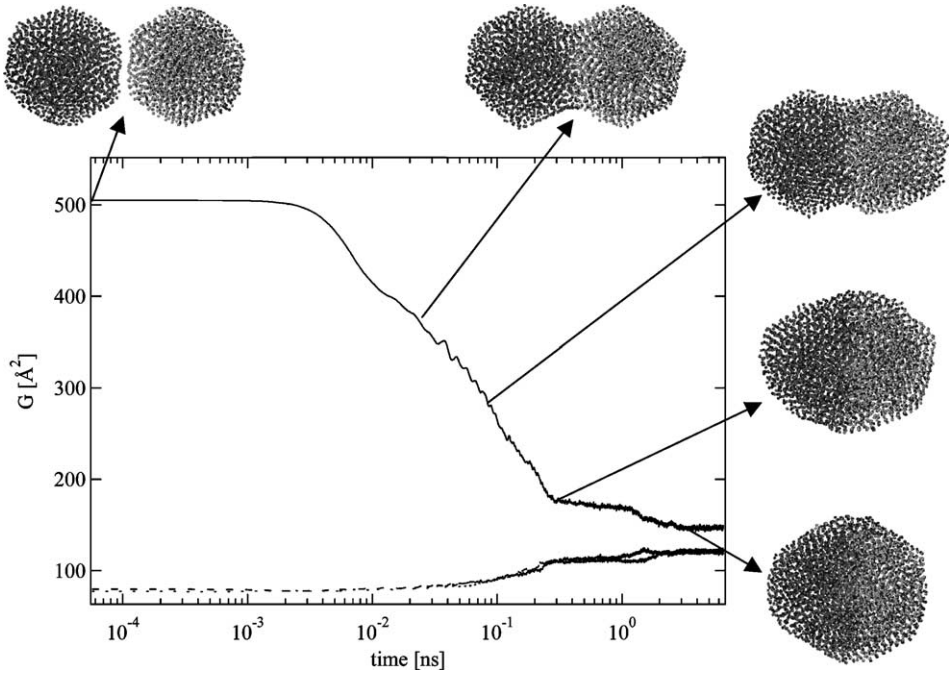

Fig. 5. Time evolution of the gyration radii in the three directions x (continuous line), y, z (dashed lines) during the sintering of two nanoparticles: $r = 20$ Å, $T = 895$ K.

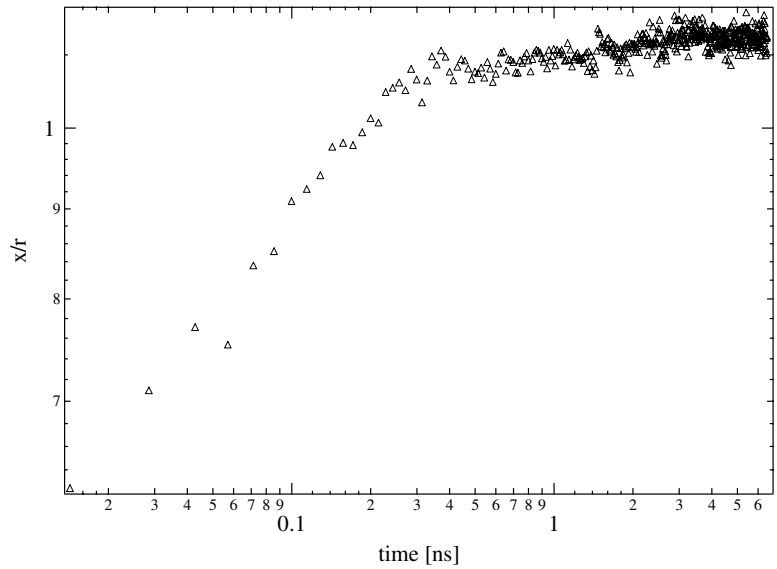

Fig. 6. Time evolution of the neck during the sintering of two nanoparticles: $r = 20$ Å, $T = 895$ K.

particles abandon in nature), because the surface energy gradient driving toward the spherical shape (minimum surface energy), may not be enough to overcome the resistance imposed by the

crystal structure of the solid. In this phase the rearrangement of the lattice structure appears to be stronger than in the first phase.

In Fig. 5 a sequence of atomic structure is also shown. The initial shape of an Au nanoparticle before the melting transition is a truncated octahedron because of the asymmetric surface energy along the index surfaces (the (1 1 1) surface has the lowest surface energy, Shim et al., 2002). This leads to a non-zero initial neck radius that will depend on the initial contact area between the two particles. This realistic situation is not covered by the assumption of two perfectly spherical particles used in the phenomenological model. During the initial transient of coalescence, the energy release due to the surface area reduction, in terms of molecular forces due to the new formed bonds, leads to an increase of the temperature of the system (Eq. (4) and Fig. 7). This behavior continues until ≈ 2 ns, i.e. until a pronounced surface area reduction is visible, as also reported in the MD simulations of silicon nanoparticles in Zachariah and Carrier (1999). Figure 7 shows also the results of the analytical model for the surface reduction and the temperature behavior for the same case. The model is predicting a faster transient for the surface area reduction (≈ 0.3 ns) and, consequently, the maximum temperature is reached faster. Moreover the maximum temperature is underestimated of ≈ 40 K. Since this is approx. 4% of the maximum temperature in the MD simulations, the agreement of the two models, analytical and numerical, is satisfactory. It has to be stressed that, as shown before, the "glue" potential is well reproducing quantitatively the properties of gold in a wide range of temperatures, so it can be taken comfortably as a reference to check the validity of the approximate macroscopic analytical formulation.

The neck growth obtained via MD and the predictions of the phenomenological model for the same particle at four different initial temperatures are depicted in Fig. 8. The results of the MD

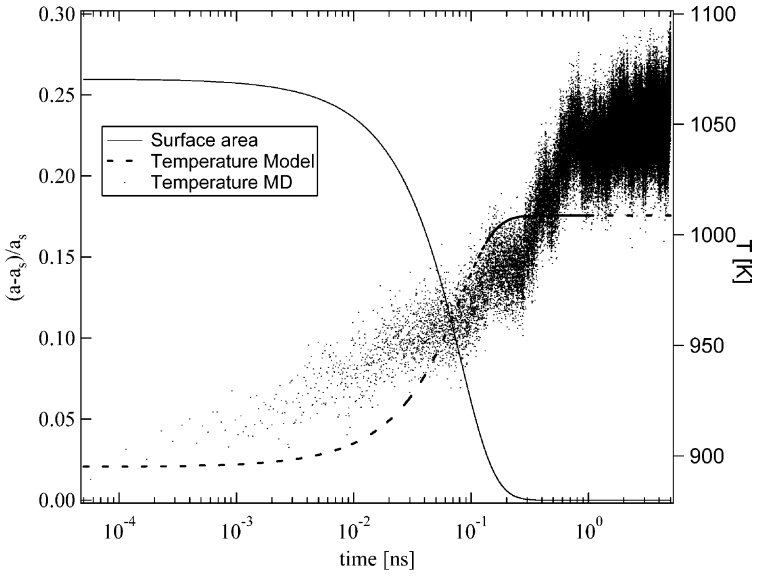

Fig. 7. Surface area reduction and temperature increase during the sintering of two nanoparticles ($r = 20$ Å, $T = 895$ K), MD simulation and analytical model.

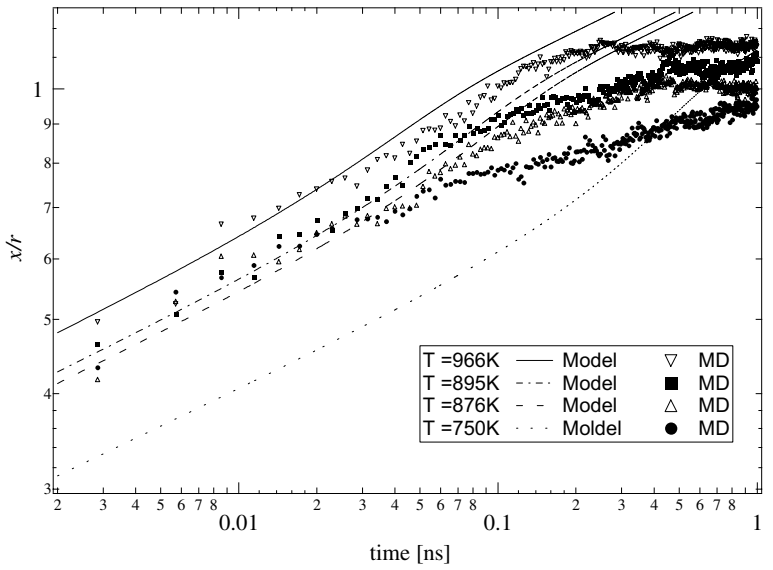

Fig. 8. Time evolution of neck growth evaluated via MD simulations and the analytical model for different temperatures and $r = 20$ Å.

simulations are giving almost parallel curves, within the accuracy of the neck evaluation calculation, except for the lower temperature case. This case exhibits an early transient phase for the neck growth, that is as fast as that of the higher temperatures. However, later, after the neck practically disappears, the growth of region where the neck was, slows down compared to higher temperatures. It seems that for the specific case under consideration, the initial temperature is not the dominant parameter for early coalescence. The phenomenon at this stage could also be influenced by the potential gradient due to the cusp at the contact point, as discussed in Zeng et al. (1998). All the curves finally reach a plateau that has lower values for lower initial temperatures. This means that the final shape of the particle is more deformed at lower temperatures, because the solid diffusion time scales required bringing the particle to a spherical shape are lager at lower temperatures. As a comparison, the asymptotic value of x/r for a final spherical shape can be evaluated assuming that the total volume of the two initial particles is equal to the volume of the final particle; finally $(x/r)_{\text{spherical}} = \sqrt[3]{2}$.

The analytical model yields acceptable results for the three higher temperature cases and provides good approximations for the corresponding sintering time. Similar results are obtained for larger particles ($r = 22.3$ and 25.2 Å), not shown here for brevity.

On the other hand, it seems that the initial temperature does not play a crucial role for smaller particles for all the studied cases. Figure 9a reports the neck growth for the sintering of two particles of 15.3 Å radius at different initial temperatures. All the MD results are packed within a small range while the analytical model is predicting a stronger temperature influence. The trend is more distinct when going to even smaller particles (Fig. 9b). The agreement between the model and the MD simulation deteriorates in accuracy signifying that at these scales other mechanisms rather than grain boundary or surface diffusion, strongly dependent on the particle temperature, have to be taken into account in the formulation of the macroscopic problem.

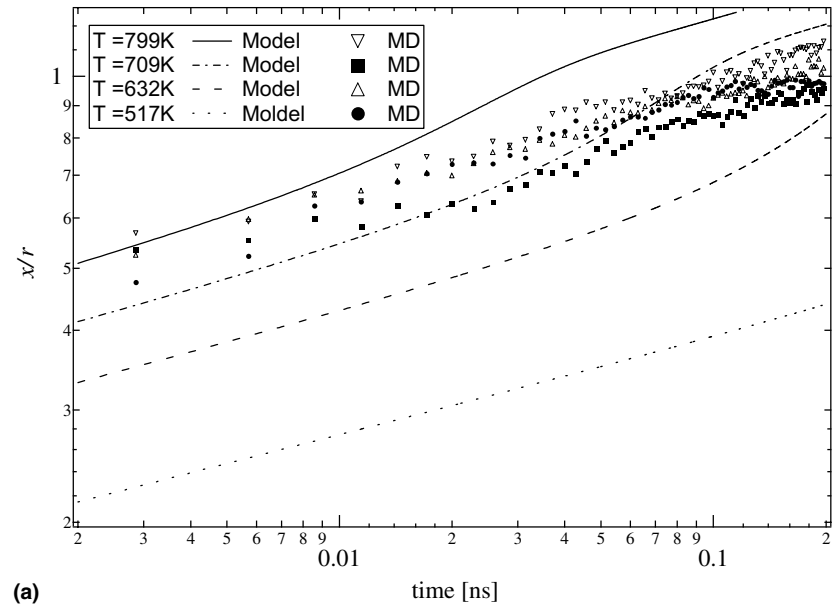

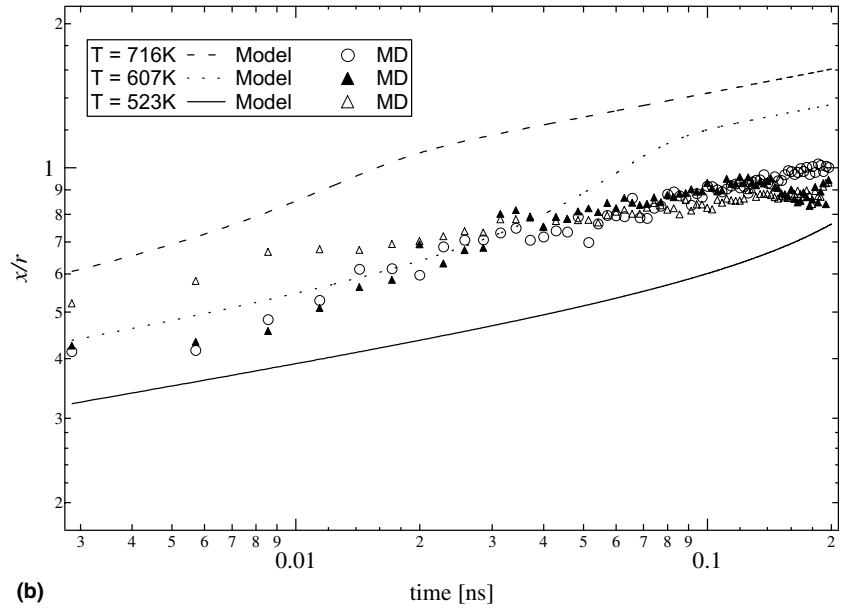

Fig. 9. Time evolution of neck growth evaluated via MD simulations and the analytical model for different temperatures: (a) $r = 15.3$ Å, (b) $r = 13$ Å.

The influence of initial lattice orientation is studied by simulating two cases of two particles of the same radius (22.3 Å) at a temperature of 938 K with different orientation. In one simulation the copied particle is only translated with respect to the original. In the other, it is also rotated anticlockwise by 45°. The two initial configurations are depicted in the first frames of Fig. 10a

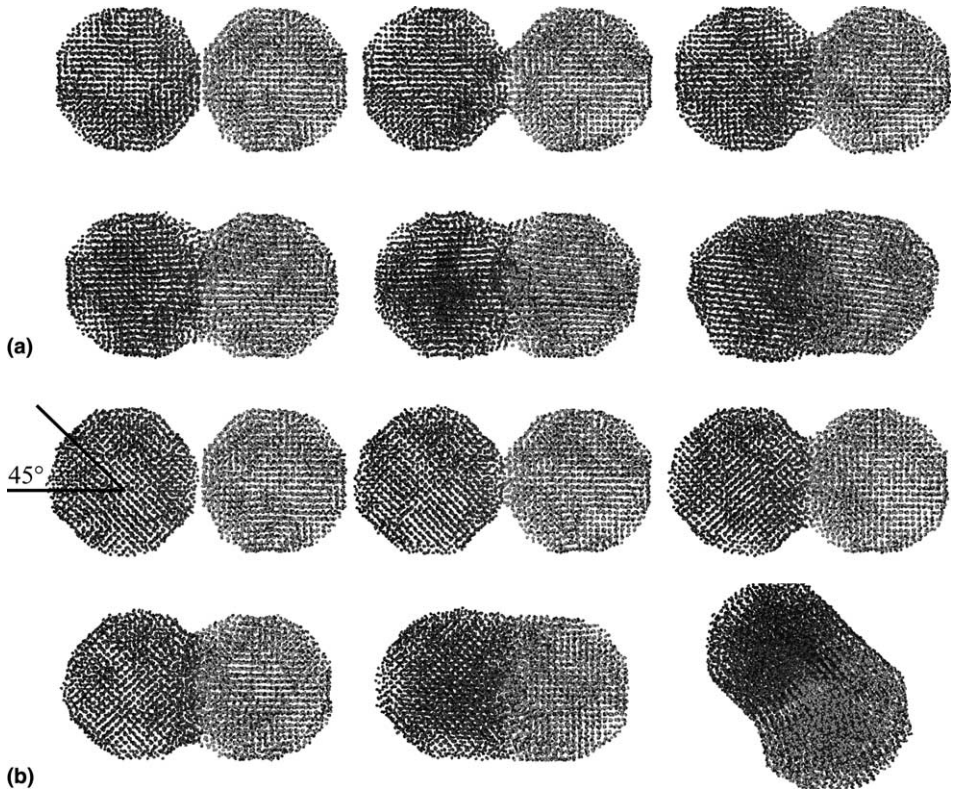

Fig. 10. Comparison of the sintering of two nanoparticles with a radius of 22.3 Å and an initial temperature of 938 K, between two different initial lattice orientations. The time distance between two frames is not constant.

and b. Both sintering processes (Fig. 10) are evolving in a similar manner as described above. However, the initial setting has an influence on the entire transient. The sintering case in which one particle is rotated presents a smaller initial contact area between the two particles. This is visible looking from the top onto the system shown in Fig. 10b, but it is not reported for brevity. The particles having initially a larger contact area and therefore a smaller potential gradient are evolving slower than the ones having a smaller contact area (Fig. 11). The same figure reports the prediction of the phenomenological model that is providing the trend of the neck growth. Fig. 10a shows the sintering of the two particles with the same lattice orientation. During neck formation, small lattice rearrangement begins and the two particles have a small relative rotation. This behavior was observed in previous works both experimental on Au nanoparticles (Iijima and Ajayan, 1991) and numerical on Cu nanoparticles (Zhu and Averback, 1996a,b) and on Au/Cu nanoparticles (Zeng et al., 1998) and seems to be another path for boundary elimination in nanoscales. The rotation is even stronger when the initial lattice arrangement of the particles is very different (Fig. 10b). After the neck is filled, the resulting particle starts slowly rotating in the simulation domain. Generally this occurrence of rotation is observed in other simulations in the present paper, especially when the temperature is well below the melting point, we speculate that the mechanical stresses within the particle due to the vivid atomic rearrangement are large enough to cause rotation of the particle as a whole.

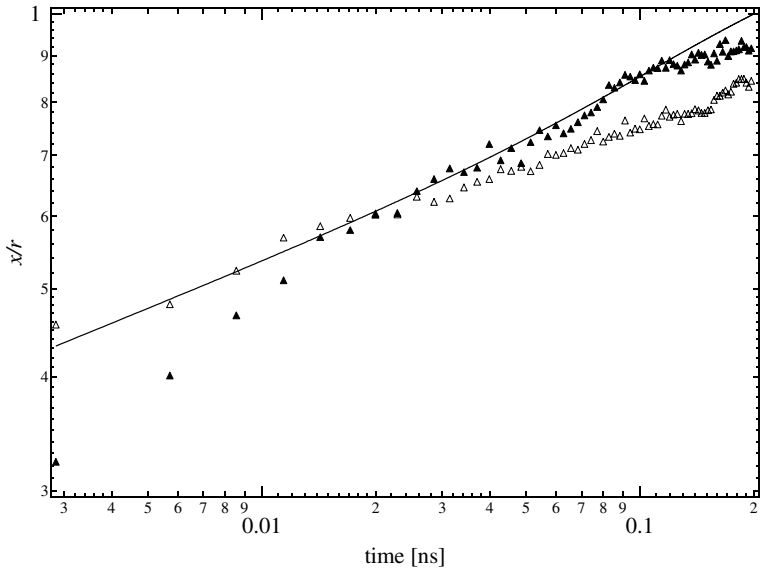

Fig. 11. Comparison of the neck growth for the sintering of two nanoparticles ($r = 22.3$ Å, $T = 938$ K), between two different initial lattice orientations. Triangles: same lattice orientation, closed triangles: 45° rotation. Solid line phenomenological model.

Before closing, a comment is made as to the effect of particle size for a fixed temperature on the phenomenon under investigation in this paper. We selected to study particles in the neighborhood of the melting temperature because this is where the interesting physics takes place. One could, for approximately the same temperature, (the temperatures are averages of a fluctuating temperature field and it is difficult to construct particles of different sizes equilibrated at exactly the same temperature), look at other particles sizes (say larger, to exemplify). However, unlike the behavior of bulk material, these particles would have significantly higher melting temperatures and no melting would occur, which is outside the interest of this work.

4. Conclusion

In this paper we reported MD simulations of gold nanoparticle melting and coalescence phenomena. The obtained results for single particle calculation were compared with earlier empirical-theoretical formulations showing that the MD approach is a reliable method to study such nanoscale phenomena. As a second step the coalescence of two nanoparticles was studied. The MD calculations improved our understanding the basics of the process such as the driving mechanisms acting at different particle sizes. For larger particles, i.e. with a radius greater than 20 Å, it can be assumed that grain boundary diffusion is dominant as the correspondence between the analytical and MD calculations is indicating. For the cases with an initial temperature near the particle melting, a good agreement between MD results and the predictions of a macroscopic phenomenological model, that was modified to account for the curvature dependence of the

particle melting temperature, was found. On the other hand, for smaller particles the model does not hold. The initial temperature seems not to play an important role and choosing between temperature dependent mechanisms, such as grain boundary or surface diffusion, does not improve the predictions of the phenomenological model. As also reported in previous works for other materials as well, the relative rotation of the particles could be another route to nanoscale boundary elimination during coalescence.

Acknowledgements

This work was supported in part by the Forschungskommission of ETH and the Swiss National Science Foundation (Grant no. 2000-063580.00).

References

Bieri, N.R., Haferl, S.E., Poulikakos, D., Grigoropoulos, C.P., 2002. Manufacturing of electrically conductive microstructures by dropwise printing and laser curing of nanoparticle-suspensions. IMECE2002, 2002 ASME International Mechanical Engineering Congress and Exposition, New Orleans, Louisiana, USA.

Bieri, N.R., Chung, J., Haferl, S.E., Poulikakos, D., Grigoropoulos, C.P., 2003. Microstructuring by printing and laser curing of nanoparticle solutions. Applied Physics Letters 82, 3529–3531.

Buffat, P., Borel, J.P., 1976. Size effect on the melting temperature of gold particles. Physical Review A 13, 2287–2298.

Chushak, Y., Bartell, L.S., 2001. Molecular dynamics simulations of the freezing of gold nanoparticles. European Physical Journal D 16, 43–46.

Coblenz, W.S., Dynys, J.M., Cannon, R.M., Colde, R.L., 1980. Initial stage solid state sintering models. A critical analysis and assessment. Materials Science Research 13, 141–157.

Ercolessi, F., Parrinello, M., Tosatti, E., 1988. Simulation of gold in the glue model. Philosophical Magazine A-Physics of Condensed Matter Structure Defects and Mechanical Properties 58, 213–226.

Ercolessi, F., Andreoni, W., Tosatti, E., 1991. Melting of small gold particles—mechanism and size effects. Physical Review Letters 66, 911–914.

Foiles, S.M., Baskes, M.I., Daw, M.S., 1986. Embedded-atom-method functions for the fcc metals Cu, Ag, Au, Ni, Pd, Pt, and their alloys. Physical Review B 33, 7983–7991.

Friedlander, S.K., Wu, M.K., 1994. Linear rate law for the decay of the excess surface-area of a coalescing solid particle. Physical Review B 49, 3622–3624.

Gjostein, N.A., 1972. Short circuit diffusion. In: Diffusion. American Society for Metals (ASM), Metals Park, Ohio, pp. 241–274.

Herring, C., 1950. Diffusional viscosity of a polycrystalline solid. Journal of Applied Physics 21, 437–445.

Iijima, S., Ajayan, P.M., 1991. Substrate and size effects on the coalescence of small particles. Journal of Applied Physics 70, 5138–5140.

Kobata, A., Kusakabe, K., Morooka, S., 1991. Growth and transformation of TiO_2 crystallites in aerosol reactor. AIChE Journal 37, 347–359.

Koch, W., Friedlander, S.K., 1990. The effect of particle coalescence on the surface-area of a coagulating aerosol. Journal of Colloid and Interface Science 140, 419–427.

Kofman, R., Cheyssac, P., Aouaj, A., Lereah, Y., Deutscher, G., Bendavid, T., Penisson, J.M., Bourret, A., 1994. Surface melting enhanced by curvature effects. Surface Science 303, 231–246.

Kruis, F.E., Kusters, K.A., Pratsinis, S.E., Scarlett, B., 1993. A simple-model for the evolution of the characteristics of aggregate particles undergoing coagulation and sintering. Aerosol Science and Technology 19, 514–526.

Lai, S.L., Guo, J.Y., Petrova, V., Ramanath, G., Allen, L.H., 1996. Size-dependent melting properties of small tin particles: nanocalorimetric measurements. Physical Review Letters 77, 99–102.

Lehtinen, K.E.J., Zachariah, M.R., 2001. Effect of coalescence energy release on the temporal shape evolution of nanoparticles. Physical Review B 63, art. no. 205402.

Lehtinen, K.E.J., Zachariah, M.R., 2002. Energy accumulation in nanoparticle collision and coalescence processes. Journal of Aerosol Science 33, 357–368.

Lewis, L.J., Jensen, P., Barrat, J.L., 1997. Melting, freezing, and coalescence of gold nanoclusters. Physical Review B 56, 2248–2257.

Mazzone, A.M., 2000. Coalescence of metallic clusters: a study by molecular dynamics. Philosophical Magazine B-Physics of Condensed Matter Statistical Mechanics Electronic Optical and Magnetic Properties 80, 95–111.

Murr, L.E., 1975. Interfacial Phenomena in Metals and Alloys. Addison-Wesley Publishing Company, Inc.

Nakaso, K., Shimada, M., Okuyama, K., Deppert, K., 2002. Evaluation of the change in the morphology of gold nanoparticles during sintering. Journal of Aerosol Science 33, 1061–1074.

Nichols, F.A., Mullins, W.W., 1965. Morphological changes of a surface of revolution due to capillarity-induced surface diffusion. Journal of Applied Physics 36, 1826–1835.

Shim, J.H., Lee, B.J., Cho, Y.W., 2002. Thermal stability of unsupported gold nanoparticle: a molecular dynamics study. Surface Science 512, 262–268.

Shimada, M., Seto, T., Okuyama, K., 1994. Size change of very fine silver agglomerates by sintering in a heated flow. Journal of Chemical Engineering of Japan 27, 795–802.

Tsantilis, S., Briesen, H., Pratsinis, S.E., 2001. Sintering time for silica particle growth. Aerosol Science and Technology 34, 237–246.

Xing, Y., Rosner, D.E., 1999. Prediction of spherule size in gas phase nanoparticle synthesis. Journal of Nanoparticle Research 1, 277–291.

Zachariah, M.R., Carrier, M.J., 1999. Molecular dynamics computation of gas-phase nanoparticle sintering: a comparison with phenomenological models. Journal of Aerosol Science 30, 1139–1151.

Zeng, P., Zajac, S., Clapp, P.C., Rifkin, J.A., 1998. Nanoparticle sintering simulations. Materials Science and Engineering A-Structural Materials Properties Microstructure and Processing 252, 301–306.

Zhu, H.L., Averback, R.S., 1996a. Sintering of nano-particle powders: simulations and experiments. Materials and Manufacturing Processes 11, 905–923.

Zhu, H.L., Averback, R.S., 1996b. Sintering processes of two nanoparticles: a study by molecular-dynamics. Philosophical Magazine Letters 73, 27–33.